Miner Petrol (2016) 110:11–27
DOI 10.1007/s00710-015-0416-0

ORIGINAL PAPER

Strontium isotope systematics of scheelite and apatite from the Felbertal tungsten deposit, Austria – results of in-situ LA-MC-ICP-MS analysis

Michael Kozlik[1] · **Axel Gerdes**[2] · **Johann G. Raith**[1]

Received: 8 May 2015 / Accepted: 25 November 2015 / Published online: 16 December 2015

Abstract The in-situ Sr isotopic systematics of scheelite and apatite from the Felbertal W deposit and a few regional Variscan orthogneisses ("Zentralgneise") have been determined by LA-MC-ICP-MS. The $^{87}Sr/^{86}Sr$ ratios of scheelite and apatite from the deposit are highly radiogenic and remarkably scattering. In the early magmatic-hydrothermal scheelite generations (Scheelite 1 and 2) the $^{87}Sr/^{86}Sr$ ratios range from 0.72078 to 0.76417 and from 0.70724 to 0.76832, respectively. Metamorphic Scheelite 3, formed by recrystallisation and local mobilisation of older scheelite, is characterised by even higher $^{87}Sr/^{86}Sr$ values between 0.74331 and 0.80689. Statistics allows discriminating the three scheelite generations although there is considerable overlap between Scheelite 1 and 2; they could be mixtures of the same isotopic reservoirs. The heterogeneous and scattering $^{87}Sr/^{86}Sr$ ratios of the two primary scheelite generations suggest modification of the Sr isotope system due to fluid-rock interaction and isotopic disequilibrium. Incongruent release of ^{87}Sr from micas in the Early Palaeozoic host rocks of the Habach Complex contributed to the solute budget of the hydrothermal fluids and may explain the radiogenic Sr isotope signature of scheelite. Spatially resolved analyses revealed isotopic disequilibrium even on a sub-mm scale within zoned Scheelite 2 crystals indicating scheelite growth in an isotopic dynamical hydrothermal system. Zoned apatite from the W mineralised Early Carboniferous K1-K3 orthogneiss in the western ore field yielded $^{87}Sr/^{86}Sr$ of 0.72044–0.74514 for the cores and 0.74535–0.77937 for the rims. Values of magmatic apatite cores from the K1-K3 orthogneiss are comparable to those of primary Scheelite 1; they are too radiogenic to be magmatic. The Sr isotopic composition of apatite cores was therefore equally modified during the hydrothermal mineralisation processes, therefore supporting the single-stage genetic model in which W mineralisation is associated with the intrusion of the K1-K3 metagranitoid at Felbertal. The subsequent regional metamorphic overprint of the deposit caused redistribution of ^{87}Sr as a consequence of metamorphic reactions involving Rb and Sr-bearing minerals. Metamorphic Scheelite 3 and apatite rims (e.g., in the K1-K3 orthogneiss) generally became more radiogenic during this process. However, local recrystallisation of primary scheelite under closed conditions (without addition of ^{87}Sr by the metamorphic fluid) is also documented. The latter process resulted in a homogenisation of the isotope composition of Scheelite 3. Further increase in $^{87}Sr/^{86}Sr$ ratios in Scheelite 3 and apatite rims is attributed to Late Alpine (?) metamorphic recrystallisation and redistribution of ^{87}Sr by metamorphic fluids.

Editorial handling: D. Frei

Electronic supplementary material The online version of this article (doi:10.1007/s00710-015-0416-0) contains supplementary material, which is available to authorized users.

✉ Michael Kozlik
michael.kozlik@gmx.at

[1] Department of Applied Geosciences and Geophysics, Montanuniversität Leoben, Peter Tunner Straße 5, 8700 Leoben, Austria

[2] Institute of Geosciences, Mineralogy, Johann Wolfgang von Goethe University, Altenhöferallee 1, 60438 Frankfurt, Germany

Introduction

The geochemical and isotopic composition of magmatic and hydrothermal minerals contains essential information on their respective crystallisation history and may provide essential insight into ore forming processes. Especially with respect to fluid-rock interaction at elevated temperatures which is an

important process that influences the enrichment, depletion or redistribution of elements in the crust and controls the development of hydrothermal ore deposits (Glodny and Grauert 2009). Thus, REE systematics and Sm-Nd isotopic characteristics of hydrothermal scheelite and apatite in ore deposits have been used to constrain the origin and evolution of mineralising fluids in W-skarns (Raimbault et al. 1993) and orogenic Au deposits (Ghaderi et al. 1999; Brugger et al. 2000; Voicu et al 2000; Dostal et al. 2009). Furthermore, the Sr isotopic systematics of scheelite provides additional valuable information on the path, source and mixing of hydrothermal fluids in orogenic Au deposits (Bell et al. 1989; Mueller et al. 1991; Darbyshire et al. 1996; Voicu et al 2000; Kempe et al. 2001; Brugger et al. 2002). Yet only sparse data exist in terms of the $^{87}Sr/^{86}Sr$ isotopic variation of scheelite in structurally controlled vein-type W-(Sb-Au), or skarn-type and stratabound W-(Mo) deposits (Eichhorn et al. 1997; Peng and Frei 2004; Tornos et al. 2008; Song et al. 2014).

Scheelite and apatite are ideal minerals to record the initial $^{87}Sr/^{86}Sr$ distribution of the respective source because both minerals can incorporate significant amounts of Sr in substitution for Ca, but only contain negligible quantities of Rb (Bell et al. 1989; Creaser and Gray 1992). Hence, ^{87}Sr produced in scheelite and apatite by the radioactive decay of ^{87}Rb is insignificant and the measured $^{87}Sr/^{86}Sr$ values can be equated with initial ratios at the time of crystallisation or element redistribution.

Over the past decades numerous studies have addressed the Felbertal scheelite deposit and its genesis (see review in Raith and Schmidt 2010). The deposit was initially interpreted as a syngenetic exhalative-sedimentary scheelite deposit related to Early Palaeozoic mafic volcanism (e.g., Höll 1975, 1977). However, a granite-related origin with subsequent metamorphic overprint of the Felbertal scheelite deposit is now widely accepted, but the exact timing and nature of the mineralisation is still debated. The single-stage epigenetic model ascribes ore formation exclusively to the intrusion of a Variscan highly fractionated Early Carboniferous I-type metagranitoid (K1-K3 orthogneiss) at ~340 Ma (Pestal 1983; Briegleb 1987, 1991; Raith and Stein 2006). According to this model, magmatic hydrothermal W-rich fluids of granitic origin caused W mineralisation in the Felbertal area and formed disseminated to stock-work type scheelite-quartz mineralisation at 340 Ma. On the contrary, Eichhorn et al. (1999) and Höll and Eichhorn (2000) argue for a two-stage genetic model in which a first stage of scheelite (Scheelite 1) formation is linked to the emplacement of differentiated granitoids at around 525 Ma. According to these authors only the second mineralisation stage (Scheelite 2) at Felbertal is linked to the intrusion of the aforementioned Variscan metagranitoid. From a geochemical point of view, both Early as well as Late Palaeozoic orthogneisses would therefore conform to the requirements crucial for granite-related scheelite mineralisation (Höll and Eichhorn 2000).

The objectives of this paper are (1) to present new in-situ Sr isotope data of scheelite and apatite from the Felbertal W deposit and two Variscan orthogneisses and (2) to discuss the results in the context of granite-related ore formation and metamorphic processes. The new data contributes to understand the petrogenetic evolution of this unusual W deposit and constrain the origin of hydrothermal fluids precipitating scheelite in the Felbertal area.

Geological setting

The Felbertal scheelite deposit, located 8 km south of Mittersill in the province Salzburg (Austria), is situated in the central part of the Tauern Window (Fig. 1) of the Eastern Alps within the Early Palaeozoic polymetamorphic Habach Complex (Frasl 1958). In general, the Habach Complex represents a polymetamorphic succession of basic to ultrabasic plutonic and volcano-sedimentary rocks with intercalations of felsic lithologies that constitute the pre-Variscan basement of the central Tauern Window (Höck 1993). The Habach Complex can be subdivided from bottom to top into the basal schist unit, the magmatic rock sequence, and the Habach phyllite (Höll 1975; Höck 1993). The basal schist unit is characterised by a metasedimentary sequence and minor intercalations of metavolcanic rocks deposited in a volcanic arc setting (Gilg et al. 1989). U-Pb dating of detrital zircons from the metasediments yielded a Late Devonian to Early Carboniferous maximum sedimentation age, thus suggesting that the basal schist unit already forms part of the Variscan basement sequence in the Habach Complex (Kebede et al. 2005).

The Felbertal scheelite deposit is restricted to the lower parts of the magmatic rock sequence (LMS) in the Felbertal area, which is interpreted as the subvolcanic part of an ophiolite (Höck 1993). It mainly comprises fine- to coarse grained amphibolites, hornblendites, various gneisses, schists, and quartz-rich rocks. Eichhorn et al. (1999) reported U-Pb SHRIMP ages of zircons from the fine-grained amphibolites (meta-basalts) of 547 ± 27 Ma. Zircons from the coarse-grained amphibolites (meta-gabbros) record an age of 482 ± 5 Ma (Eichhorn et al. 2001) and conventional U-Pb dating of zircons from the hornblendites (meta-cumulates?) yielded a crystallisation age of 496 ± 2 Ma (von Quadt 1992). Volcanic arc-related calc-alkaline I-type granitoids were emplaced during the Cambrian (Höll and Eichhorn 2000). An Early Cambrian age of these orthogneisses is confirmed by U-Pb SHRIMP dating of zircons from the "EOZ gneiss" (orthogneiss underlying the scheelite-rich quartzite in the Eastern Ore Zone), yielding a magmatic formation age of 529 ± 17 Ma (Eichhorn et al. 1999).

The uppermost tectonic unit within the Habach Complex is the Habach phyllite, a sequence of dark phyllites, micaschists,

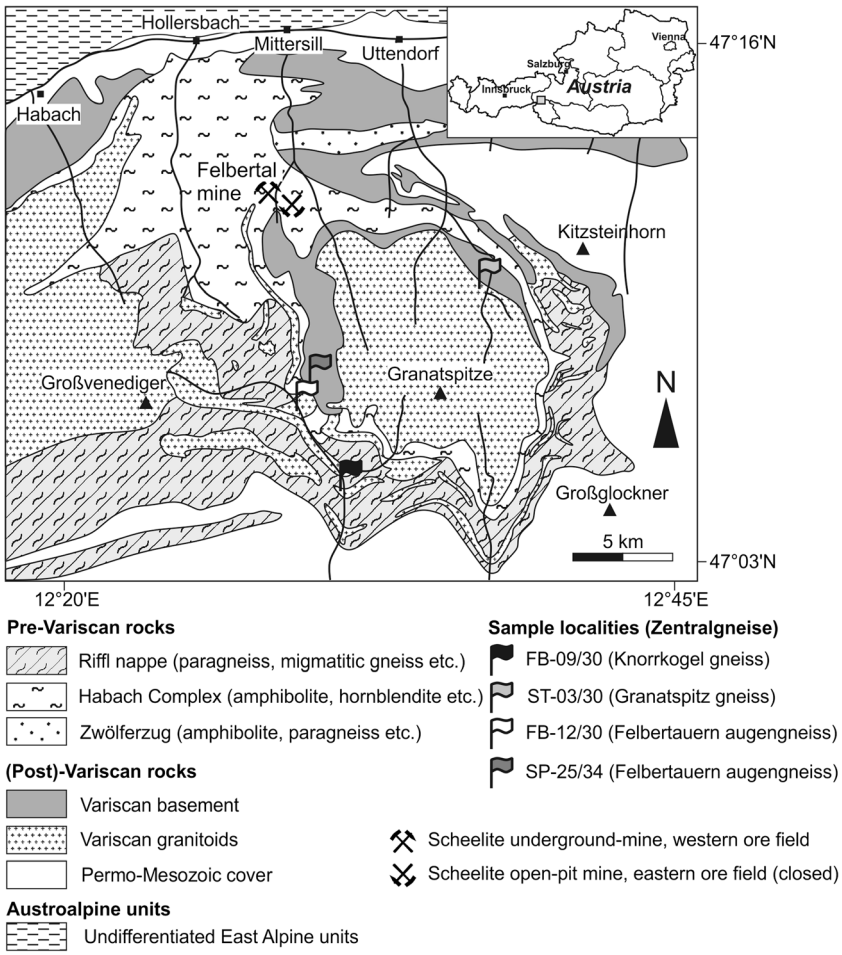

Fig. 1 Generalised geological map of the central Tauern Window showing the location of the Felbertal W deposit (modified from Höll and Eichhorn 2000; Kebede et al. 2005; Raith and Stein 2006)

and mafic to felsic metavolcanics that were deposited in a volcanic arc environment (Eichhorn et al. 1999). Zircons from gabbro clasts in a metamorphosed volcano-clastic agglomerate in the Habach phyllite yield an upper intercept age of 536 ± 8 Ma, suggesting an Early Cambrian protolith age (Kebede et al. 2005). A nearly concordant age of 506 ± 9 Ma obtained from a rounded detrital zircon generation from the same rock is interpreted as the maximum sedimentation age of the Habach phyllite (Kebede et al. 2005).

Early Carboniferous to Early Permian granitoids – referred to as Zentralgneise – intruded this Cambro-Ordovician basement sequence as a consequence of the accretion of peri-Gondwana terranes and the subsequent collision of Gondwana with Laurasia (Stampfli and Borel 2002). These metagranitoids occur in the central part of the Tauern Window either as large voluminous plutons forming dome-like structures (e.g., Granatspitz gneiss) or as elongated sill-like orthogneiss bodies (e.g., Felbertauern augengneiss). Eichhorn et al. (2000) distinguished four distinct pulses of granitoid melt generation in the central Tauern Window in the Middle Devonian, Early Carboniferous, Late Carboniferous, and Early Permian, respectively. Magmatism is linked to an evolving Variscan collisional belt starting with an active plate margin setting in the Middle Devonian, generating subduction-related, volcanic arc granites (e.g., Zwölferkogel gneiss: 374 ± 10 Ma, Eichhorn et al. 2000). During the Early Carboniferous, collisional I-type granites and anatexites were produced in a transpressional tectonic regime as the result of the amalgamation of Gondwana and Laurasia (e.g., Felbertauern augengneiss: 340 ± 4 Ma, Eichhorn et al. 2000). After a period of exhumation and erosion, a third pulse of granitoid magmatism generated late-Variscan calc-alkaline I-type melts (e.g., Peitingalm gneiss: 300 ± 5 Ma, Eichhorn et al. 2000). The subsequent change to an extensional tectonic setting caused post-Variscan granitoid formation during the Early Permian, with the intrusion of a large S-type batholith (Granatspitz gneiss: 271 ± 4 Ma, Eichhorn et al. 2000). However, the age of this batholith is debated; Kebede et al. (2005) postulated an emplacement age of 314 ± 1 Ma for this metagranitoid.

The central Tauern Window was affected by Alpine regional metamorphism reaching lower amphibolite facies conditions (500–590 °C, 4.5–7.0 kbar) during the Late Eocene/Oligocene in its center (see Grundmann 1989; Höll and Eichhorn 2000 and references therein). The Late Alpine metamorphism has been regarded as the dominant regional

metamorphic event in the Tauern Window, although the question of the extent of a pre-Alpine metamorphic overprint in the Felbertal area is still awaiting a final answer. Eichhorn et al. (1995) argued that in the Felbertal deposit Variscan metamorphism was higher grade (T_{max} = 590 °C) than the Alpine upper greenschist- to amphibolite-facies metamorphic event (T_{max} = 520 °C). Accordingly, the dominant fabrics at the Felbertal scheelite deposit are regarded as Variscan, although the stacking of the distinct nappes/tectonic slices is attributed to Alpine compressional tectonics (Höll and Eichhorn 2000). Other support for a Variscan age of metamorphism comes from Re-Os molybdenite ages from the Felbertal W deposit, ranging between 358 and 336 Ma (Raith and Stein 2006) and a rather imprecise Sm-Nd age of metamorphic Scheelite 3 yielding 319 ± 34 Ma (Eichhorn et al. 1997). Conversely, Koller and Richter (1984) reported lower Variscan (?) *P-T* conditions of 420 °C and 2 kbar for the Habach Complex. The Alpine metamorphic stage is recorded by a Sm-Nd isochron age of Scheelite 4 (see below) yielding 29 ± 17 Ma (Eichhorn et al. 1997).

Tungsten mineralisation

An eastern (open pit) and a western (underground) ore field, which are slightly displaced relative to each other, probably as the result of an Alpine dextral, west-dipping, thrust-slip fault, are distinguished in the Felbertal area (Höll and Eichhorn 2000). Today, active mining is limited to the western ore field. The W-mineralisation in the Felbertal mine is generally of pervasive nature throughout the different lithologies; economic grades are commonly associated with quartz veins in a stock-work like mineralisation. The mineral assemblage of the veins includes quartz, scheelite and minor to accessory muscovite, epidote, clinozoisite, zoisite, calcite, fluorite, phenakite, beryl, titanite, Nb-Ta-minerals, molybdenite, pyrite, pyrrhotite, and chalcopyrite. Moreover, a variety of rare Pb-Bi-sulfosalts occurs within the quartz veins (Topa et al. 2002 and references therein).

The Early Palaeozoic sequence, constituting the host rocks of the scheelite ores, was intruded by a highly differentiated leucocratic metagranitoid during the Early Carboniferous (U-Pb zircon concordia age of 336 ± 19 Ma, Eichhorn et al. 1995). This orthogneiss, referred to as K1-K3 orthogneiss in the mine, is mainly exposed underground in the western ore field where it was spatially linked to (now mined) high-grade mineralisation (parts of the K1 and K3 ore bodies). This orthogneiss is regarded as the source of the W mineralisation according to the single-stage epigenetic model (Pestal 1983; Briegleb 1987, 1991; Raith and Stein 2006). A striking feature of the K1-K3 orthogneiss is its high concentrations of Nb, Ta, Be, Rb, U, Mo, Bi, F, and W. The orthogneiss can be classified as a felsic metaluminous to weakly peraluminous high K calc-alkaline I-type syeno- monzogranite mainly composed of quartz, albite, potassium feldspar and varying amounts of biotite and phengitic muscovite (Finger et al. 1985; Höll and Eichhorn 2000; Kozlik and Raith 2014). Primary magmatic accessory minerals are zircon, apatite and relicts of titanite and allanite; the latter is commonly surrounded by a metamorphic clinozoisite-epidote corona.

Based on optical, petrographic, geochemical, and geochronological criteria, four scheelite generations are distinguished (Höll 1975; Schenk 1990; Eichhorn et al. 1997):

Scheelite 1 is very fine-grained (<0.4 mm), colourless though yellowish-white fluorescent in short-waved UV light. A remarkable feature is the fine-scale oscillatory growth zoning revealed in cathodoluminescence (CL) images (Fig. 2a). Its Mo content does not exceed 1.8 mass% and it has been the most prominent generation in the eastern ore field of the Felbertal scheelite deposit where it occurred in mylonitic (?) laminated scheelite-quartz ores. Eichhorn et al. (1999) had postulated a Cambrian formation age for this scheelite generation linked to these pre-Variscan orthogneisses (520–530 Ma), but recent in-situ U-Pb dating of Scheelite 1 by LA-SF-ICP-MS yielded a concordia age of 335.5 ± 4.6 Ma (Raith et al. 2011). corroborating its genetic relationship with the Early Carboniferous K1-K3 orthogneiss.

Scheelite 2 is the common generation in the western ore field and is easily identified by its variable grain size ranging from mm- to cm-scale and its grey colour (Fig. 2b). It displays yellowish fluorescence in UV light (Fig. 2c, d) and Mo contents are similar to Scheelite 1 (Eichhorn et al. 1997). Large Scheelite 2 crystals occasionally show a weakly developed growth zoning that is visible only in CL images. The occurrence of micro-fractures in Scheelite 2 filled with Scheelite 3 is indicative of recrystallisation under transitional brittle-ductile deformation; in high-strain zones Scheelite 2 commonly forms porphyroclasts (Fig. 2d, e) intergrown with recrystallised Scheelite 3 of metamorphic origin. Quartz-scheelite veins featuring the second generation frequently crosscut the K1-K3 orthogneiss, thus an Early Carboniferous maximum crystallisation age is asserted.

Scheelite 3 formed via recrystallisation of Scheelite 1 and 2 (Fig. 2a, d, e) or crystallised as rims around the older scheelite (Fig. 2f); it also occurs in micro-fractures within these earlier generations. A bluish fluorescence colour in short-waved UV light (Fig. 2c, d), insignificant Mo contents and bright luminescence in CL (Fig. 2a, e, f) are characteristic for Scheelite 3. Diffuse zoning can be observed in some grains in CL. Eichhorn et al. (1997) calculated a Sm-Nd isochron age for Scheelite 3 of 319 ± 34 Ma which they interpreted as the time of recrystallisation of Scheelite 1 and 2 during Variscan regional metamorphism.

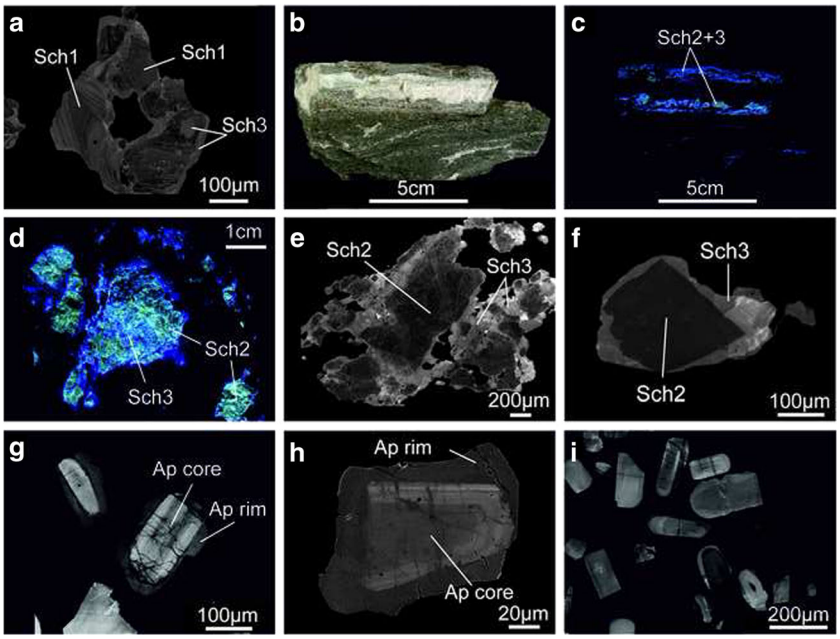

Fig. 2 Hand-specimen photographs in normal and short-wave UV light, cathodoluminescence (CL) images and back-scattered electron (BSE) images of scheelite and apatite. **a** CL image of Scheelite 1 (Sch1) with fine oscillatory zoning overgrown and partly replaced by CL-brighter metamorphic Scheelite 3 (Sch3); eastern ore field, laminated scheelite-quartz ore, sample FT-74. **b** Photograph of a fine-grained amphibolite with foliation-parallel cm thick quartz-scheelite vein; western ore field, K2 orebody level 1005 m, sample K2-1005 MB. **c** Scheelite 2 (Sch2) and Scheelite 3 (Sch3) in the same sample visible in UV light; note symmetric arrangement of scheelite at the vein selvedge. **d** Yellow fluorescent Scheelite 2 replaced by bluish fluorescent Scheelite 3; same sample. **e-f** CL images of Scheelite 2 replaced/overgrown by Scheelite 3 in a quartz-scheelite vein; western ore field level 1164 m, sample B-K1q-A. **g** CL-image of apatite in the K1-K3 orthogneiss showing bright cores with micro-fractures and dark rims; western ore field level 1065 m, sample Gn-1065b. **h** BSE image showing apatite core-rim relationships in the K1-K3 orthogneiss; western ore field level 1234 m, sample K1-1234. **i** CL-image of apatite grains from Felbertauern augengneiss; sample FB-12/30

Scheelite 4 displays white to pale-blue fluorescence, is free of Mo and forms up to several cm sized isolated porphyroblasts within Alpine metamorphic quartz veins that typically crosscut older Variscan structures including the first generation of quartz-scheelite veins. A Sm-Nd isochron age of 29 ± 17 Ma corroborates the Alpine age of Scheelite 4 and reflects local remobilisation of Variscan scheelite generations during Alpine regional metamorphism (Eichhorn et al. 1997).

Sample description

Laminated scheelite-quartz ore and gneiss (eastern ore field)

Both samples were not collected by the authors in course of this study but are from archive material of previous projects; such high-grade ores cannot be sampled any more in the abandoned open pit in the eastern ore field. Scheelite 1 was analysed in two sub-samples of sample FT-74, one polished thin section and one polished section. The sample is a laminated scheelite-quartz ore from the former open pit mine in the eastern ore field. In the past this ore type has been described as scheelite-rich quartzite ("Scheelitreicherz"; Höll 1975). Scheelite (Scheelite 1 and 3) is very fine-grained (<0.4 mm) and strongly aligned, causing a prominent foliation in this high-grade ores. Saccharoidal quartz, the major mineral, is completely recrystallised. In contrast, scheelite shows incomplete recrystallisation. Stringers of very fine-grained scheelite aggregates are composed of recrystallised blue-fluorescent Scheelite 3 plus slightly larger elongated relicts of yellow-white fluorescent Scheelite 1. Relicts of the latter preserve fine oscillatory growth zoning (Fig. 2a). White mica occurs as an accessory mineral.

Additionally, Scheelite 1 and apatite were analysed from a leucocratic, laminated, scheelite-rich gneiss from the eastern ore field (sample FS-1). FS-1 differs from the laminated scheelite-quartz ore in that it contains more plagioclase, muscovite, epidote, apatite and zircon but less quartz. However, FS-1 features an elevated grade of the fine-grained first scheelite generation.

K1-K3 orthogneiss (western ore field)

The K1-K3 orthogneiss samples studied are from the levels 1152, 1100, 1065, and 725 m in the operating underground

mine. Additionally, a weakly mineralised aplitic gneiss sample was taken on level 1124 m. The latter represents the most fractionated member of the K1-K3 orthogneiss (Kozlik and Raith 2014). Scheelite 2 and 3 occurs either in mm to cm thick quartz veinlets or disseminated throughout the orthogneiss. Quartz and varying amounts of plagioclase, potassium feldspar, biotite, and phengitic muscovite constitute the main mineral assemblage. Zircon, titanite, allanite, clinozoisite, epidote, calcite, and apatite are common accessory phases. Usually, apatite is associated with muscovite, biotite, plagioclase, calcite, fluorite and epidote in the matrix of the orthogneiss. Apatite crystals are <150 μm and display a pronounced zoning in CL- and back-scattered electron (BSE) images allowing distinction of cores and rims (Fig. 2g, h). The cores are characterised by brighter CL signal and they tend to be euhedral. They sometimes reveal oscillatory growth zoning and usually show evidence for intense brittle deformation as indicated by a crosscutting network of micro-fractures (Fig. 2g). The rims are darker in CL, are anhedral and do not display the same intensity of brittle deformation as the cores. In addition, BSE images reveal features of resorption and dissolution-reprecipitation along the core-rim boundaries (Fig. 2h). Frequently, apatite rims are less than 20 μm in size, consequently aggravating measurements by laser ablation. Based on the textural differences we interpret the cores and rims as two distinct growth stages.

Quartz-scheelite vein (western ore field)

Quartz-scheelite veins crosscut both Early Palaeozoic host rocks as well as the K1-K3 orthogneisses in the western ore field where these veins represent the major ore type. Sample B-K1q-A (thin section) is from a quartz-scheelite vein from level 1164 m where it crosscuts the K1-K3 orthogneiss. It contains both larger grains of yellow fluorescent Scheelite 2 and blue fluorescent Scheelite 3 (Fig. 2e, f). Scheelite is associated with calcite, titanite, phenakite and blue beryl (aquamarine); the latter partly replaces phenakite or occurs as poikiloblastic crystals with inclusions of phenakite (cf., Franz et al. 1986). Occasionally, titanite is completely replaced by rutile, calcite, fluorite, and quartz. A 1 to 3 mm thick potassium feldspar veinlet containing minor albite, calcite, Nb-bearing rutile, zircon, and pyrrhotite crosscuts the quartz-scheelite vein.

Meta-quartz diorite (western ore field)

Scheelite 2 and 3 from the coarse-grained quartz dioritic biotite-albite gneiss on level 1038 m were analysed (sample Gn-1038a). The mineral assemblage is characterised by pale-brown biotite, albite, quartz, zoisite and subordinate amounts of anhedral to euhedral titanite, apatite, calcite, amphibole, and garnet. Quartz is aligned in lenticular clusters and shows significant evidence of recrystallisation. A 0.5 mm thick fluorite vein, associated with quartz and scheelite, crosscuts the sample parallel to its foliation. Scheelite 2 forms porphyroclasts (<5 mm), occasionally with well-developed growth zoning. This larger grain was used to determine the $^{87}Sr/^{86}Sr$ distribution within a single scheelite crystal (see below).

Sample Gn-1262 was taken on level 1262 m. Compared to Gn-1038a it is finer-grained and has a more pronounced schistosity. In thin section biotite displays a gradual transition from fresh, dark brown biotite to chloritized biotite and finally to chlorite. Zoisite is common and forms prismatic crystals parallel to the foliation of the rock. A 100 μm thick calcite-filled vein crosscuts the gneiss. Scheelite has not been observed. Subhedral, prismatic apatites are <150 μm and display similar pronounced core-rim textures in CL images as observed in the K1-K3 orthogneiss.

Younger K2 orthogneiss (western ore field)

In the course of a drilling campaign on the 1175 m level that aimed to drill through the K1-K3 orthogneiss body, a four meter thick leucocratic, biotite-poor gneiss was intersected. Sample AP-3.82 is from the drill core UB-343 (meter 3.82–7.53) and is characterised by the mineral assemblage plagioclase, potassium feldspar, zoisite, quartz, and biotite. Biotite is irregularly distributed indicating post-tectonic crystallisation. Common accessory minerals are muscovite, anhedral to subhedral titanite, allanite, clinozoisite, zircon, and scheelite. Clearly, post-magmatic alteration and mineralisation processes affected this orthogneiss. The sample shows evidence of potassic alteration in form of a network of thin (<200 μm) potassium feldspar veinlets. Where these small veins crosscut the gneiss, plagioclase is altered to sericite. Scheelite 2 and 3 are mainly restricted to quartz veinlets. Due to its chemical characteristics (M. Kozlik, unpublished data) this gneiss is best compared to the Cambrian gneisses ("Younger K2 orthogneiss") in the deposit. According to Eichhorn et al. (1999) these orthogneisses derived from Early Palaeozoic I-type granitoids (U-Pb SHRIMP zircon age 519 ± 14 Ma) and are associated with scheelite mineralisation (K2 ore body) in the western ore field.

Zentralgneise

Two samples of Zentralgneise, both from localities well outside the Felbertal scheelite deposit, were included in this study because they contain small amounts of scheelite. A scheelite-bearing specimen of Felbertauern augengneiss (SP-25/34) was sampled on the road to the St. Pöltener Hütte north of the Matreier Tauernhaus at 2052 m above sea level (Fig. 1). Scheelite showings in this area have already been reported from Meßelinggraben - Grüner See - Schwarzer See area,

where it was found in metabasites of the basal amphibolite member (Höll 1975, 1979; Neinavaie et al. 1983). This orthogneiss is composed of potassium feldspar crystals within a fine-grained matrix of quartz, plagioclase and biotite. Calcite, titanite, apatite, allanite, zircon, epidote, and clinozoisite are the accessory minerals.

Another sample (ST-03/30) of Zentralgneise, referred to as Granatspitz gneiss in the regional literature, was collected ~2 km northwest of Enzingerboden in Stubachtal (Fig. 1). It contains sparse scheelite mineralisation. The mineral assemblage is characterised by fine-grained quartz, biotite, muscovite, and feldspars. Plagioclase commonly contains minute inclusions of muscovite and frequently forms inclusions in potassium feldspar porphyroblasts that have overgrown the existing foliation. The metamorphic assemblage includes garnet, biotite, muscovite, quartz, and plagioclase. In both gneisses disseminated fine-grained scheelite is blue fluorescent and does not show any zoning under CL.

In addition to scheelite, apatite from the Felbertauern augengneiss (SP-25/34, FB-12/30) and Knorrkogel gneiss (FB-09/30) were analysed for $^{87}Sr/^{86}Sr$ (Fig. 1). Apatite in the Felbertauern augengneiss is euhedral to sub-rounded and shows homogeneous cores in CL with either CL-brighter or CL-darker rims (Fig. 2i). Sample FB-09/30 displays a well-developed foliation with larger potassium feldspars (<2 cm) creating an augen gneiss texture. Recrystallised quartz, plagioclase and biotite form the matrix. Biotite is partly chloritised and plagioclase features minute muscovite inclusions. Common accessory minerals are apatite, titanite, allanite, clinozoisite, epidote, and calcite.

Methods and analytical techniques

Strontium isotope measurements were performed with a Thermo-Finnigan Neptune multi collector ICP-MS at Johann Wolfgang von Goethe University Frankfurt (JWG) coupled to a Resolution S-155 193 nm ArF Excimer (Resonetics) laser system during two analytical sessions (August 2013 and June 2014). Key instrument parameters and operating conditions are listed in Table 1. The laser spot size (50–190 μm) was chosen depending on size and Sr concentration of the particular area of the individual grains. Each analysis included 25 s acquisition of background and 25–35 s of laser ablated material with an integration time of 0.52 s. Outliers were rejected based on a 2σ criterion for all data with ^{88}Sr signal >0.5 V. The instrumental mass bias for Sr isotopes was corrected using an exponential law function and a $^{86}Sr/^{88}Sr$ of 0.1194. For Rb isotopes the mass bias was corrected using the Sr mass bias of the individual integration step multiplied by a daily ascertained βSr/βRb offset factor. This offset factor was determined empirically from analyses of NIST soda-lime glass SRM 610, which was measured (130 μm spot) at the beginning and end of each analytical session. The aim was to correct the enormous isobaric interference (> 400 %) of ^{87}Rb on ^{87}Sr in case of the NBS 610. Woodhead and Hergt (2001) reported a solution mode TIMS $^{87}Sr/^{86}Sr$ ratio of 0.70969 for NBS 610. Selection of the offset factor was based on the first two SRM 610 analyses and applied to all subsequent analyses. Typical $^{87}Sr/^{86}Sr$ of SRM 610 was 3.265 before correction and 0.7093 ± 0.0008 (n = 6) afterwards. Correction of interferences of Kr isotopes (impurities in the Ar gas) on mass 84 (e.g., 0.051 V) and 86 (e.g., 0.016 V) was successfully accomplished by background subtraction. Almost all analyses yielded $^{84}Sr/^{86}Sr$ of 0.05648 after correction. Elevated rare earth element contents in apatite make it necessary to correct for isobaric interferences by doubly-charged Er and Yb isotopes (168^{2+}, 170^{2+}, 172^{2+}, 174^{2+}, and 176^{2+}) on mass 84, 85, 86, 87, and 88. This was done by monitoring the half masses 83.5, 84.5 and 86.5 and using the natural Yb and Er isotope ratios, the Sr mass bias of the individual integration step, and an empirical determined βSr/βYb offset factor. The latter was determined using the SRM 610 in the same way as described for the βSr/βRb. Typical corrections for apatite were in the range of 0.01 to 0.0001 on the $^{87}Sr/^{86}Sr$. Durango apatite was analysed to monitor and verify the accuracy of the corrections (see below).

Prior to laser measurements the Neptune instrument was tuned using 150 ppb SRM 987 solution aspirated with a standard glass spray chamber using a PFA-100 μ-flow nebulizer (Elemental Scientific). All data acquired during the subsequent analytical session were adjusted relative to the NBS 987 of $^{87}Sr/^{86}Sr$ 0.710248. Quoted uncertainties are quadratic additions of the within run precision of each analysis and the

Table 1 Key instrument parameters and operating conditions for Sr isotope determination by laser ablation

Neptune MC-ICP-MS	
RF power	1350 W
Plasma gas flow rate	15 l min^{-1}
Auxiliary gas flow rate	0.82 l min^{-1}
Interface cones	Nickel
Collectors	Faraday at $10^{-11}\Omega$
Mass resolution	400 m/z
Typical sensitivity (Total Sr solution)	90 V/μg g^{-1}
Laser ablation system (Resolution, Resonetics)	
CompexPro 102 ArF excimer	193 nm
Ablation cell	S-155
Energy density	4–5 J cm^{-2}
Helium gas flow rate	0.60 l min^{-1}
Argon gas flow rate	0.90 l min^{-1}
Effective volume	~ 1.8 cm^3
Spot size (diameter)	50–190 μm
Repetition rate	6 Hz

reproducibility of the in-house plagioclase standard MIR-a (2σ = 0.006 %, n = 15). Accuracy and daily reproducibility of the method was verified by repeated analyses of Durango apatite and MIR-a, which yielded $^{87}Sr/^{86}Sr$ of 0.70634 ± 0.00007 (2σ, n = 36) and 0.70309 ± 0.00004 (n = 29), respectively. This is in perfect agreement with previously published TIMS results (e.g., Horstwood et al. 2008; Rankenburg 2002) and the LA-MC-ICP-MS long-term average of MIR-a (0.70309 ± 0.00005; n > 100) and Durango apatite (0.70634 ± 0.00008, n > 50) at JWG.

Results

Rb-Sr data of scheelite

Scheelite 1, 2, and 3 from the distinct lithologies/ores in the eastern and the western ore field described above were analysed for their Rb-Sr isotope composition. In total 141 analyses were made on 10 samples. Additionally, scheelites from the Felbertauern augengneiss (SP-25/34) and the Granatspitz gneiss (ST-03/30) were analysed. The data are summarised in Table 2. $^{87}Sr/^{86}Sr$ values are also graphically presented in Figs. 3, 4, 5, and 6. The complete dataset is available as electronic supplementary material (Electronic appendix 1). In Scheelite 1 and 2 Sr concentrations vary in the range of several hundreds of ppm (Table 2). However, both generations usually show low Sr contents with similar median values of 78 and 73 ppm respectively, although Scheelite 2 from the Younger K2 orthogneiss (AP-3.82) yields elevated median concentrations of 191 ppm Sr. The third scheelite generation is characterised by higher Sr concentrations ranging from 27 to 949 ppm (median 206 ppm). The concentrations of Sr in scheelite from the Felbertauern augengneiss are slightly higher (159–901, median 530 ppm) compared to the Granatspitz gneiss (122–311, median 219 ppm).

Table 2 Sr isotopic data of the different scheelite stages, apatite cores and apatite rims. Abbreviations: e = eastern ore field, w = western ore field; for results of individual analyses see electronic supplementary material

			Sr [ppm]			$^{87}Rb/^{86}Sr$			$^{87}Sr/^{86}Sr_i$		
Mineral	Sample	n	Min	Max	Median	Min	Max	Median	Min	Max	Median
Scheelite											
Scheelite 1, e	FS-1 FT-74	27	39	234	78	0.00047	0.33191	0.07243	0.72078	0.76417	0.73063
Scheelite 2, w	Gn-1038a Gn-1065b K1-725 K1-1100 K1-1152 AP-1124 B-K1q-A	38	31	342	73	0.00001	0.11080	0.00172	0.70724	0.76832	0.74283
Scheelite 2, w	AP-3.82	13	68	253	191	0.00002	0.02509	0.00037	0.70775	0.71093	0.70833
Scheelite 3, w	Gn-1038a Gn-1065b K1-725 K1-1100 K1-1152 B-K1q-A	46	27	949	206	0.00001	0.86641	0.00124	0.72383	0.80689	0.77532
Scheelite 3, e	FS-1	17	27	465	210	0.00007	0.08010	0.00072	0.72610	0.76320	0.73646
Felbertauern augengneiss	SP-25/34	2	159	901	530	0.00715	0.02109	0.01412	0.77348	0.77366	0.77357
Granatspitz gneiss	ST-03/30	6	122	311	219	0.00003	0.05198	0.00598	0.74387	0.77467	0.74422
Apatite core											
K1-K3 orthogneiss, w	Gn-1065b K1-725 K1-1100	7	174	779	427	0.00019	0.00575	0.00256	0.72044	0.74514	0.72549
Scheelite-rich gneiss, e	FS-1	10	82	672	202	0.00191	0.02685	0.00620	0.72264	0.73845	0.73377
Meta-quartz diorite, w	Gn-1262	4	892	1274	1173	0	0.00267	0.00042	0.70527	0.70672	0.70586
Felbertauern augengneiss	FB-12/30SP-25/34	11	53	514	246	0.00053	0.03633	0.00283	0.71634	0.72954	0.72192
Knorrkogel gneiss	FB-09/30	11	392	1094	478	0.00043	0.01732	0.00250	0.70649	0.70896	0.70790
Apatite rim											
K1-K3 orthogneiss, w	Gn-1065bK1-725K1-1100K1-1152	8	162	1296	679	0.00016	0.07510	0.00817	0.74535	0.77937	0.77211
Meta-quartz diorite, w	Gn-1262	4	944	1248	1105	0.00002	0.00299	0.00005	0.70833	0.71061	0.70899

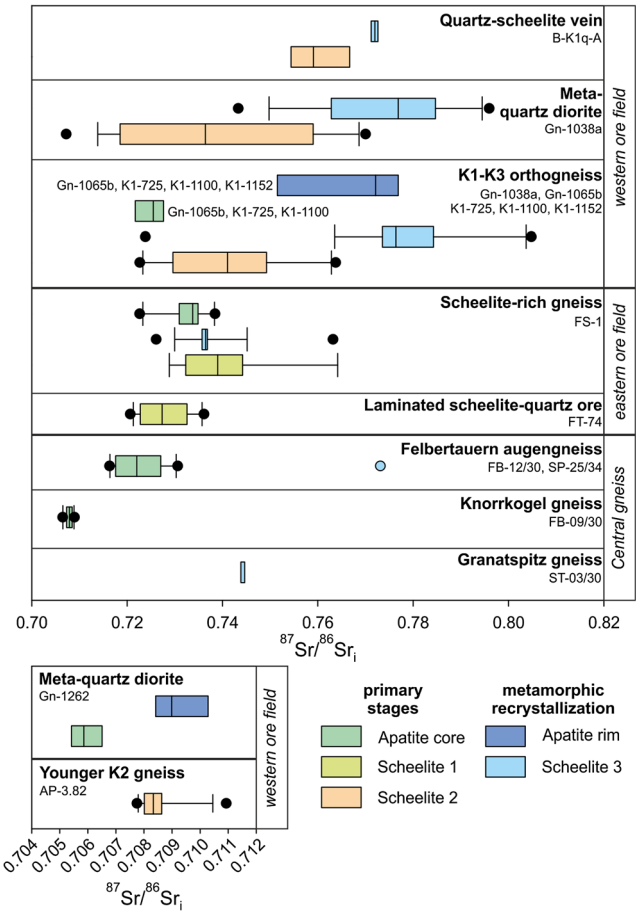

Fig. 3 Compilation of $^{87}Sr/^{86}Sr$ values in scheelite and apatite arranged in box-and-whisker diagrams according to the hosting lithologies. The boxes represent the interquartile range between the 25th and 75th percentile with the median shown as *vertical line* inside the box. The whiskers refer to the 10th and 90th percentile; individual outliers are illustrated as *black dots*. The two scheelite analyses from the Felbertauern augengneiss yielding identical $^{87}Sr/^{86}Sr$ values are shown as *light blue dot*

The median $^{87}Rb/^{86}Sr$ ratios are generally below 0.075, although a few analyses yielded more elevated ratios of up to 0.866 (Table 2); they are significantly lower in the Zentralgneise (<0.052). From the $^{87}Rb/^{86}Sr$ measurements the initial $^{87}Sr/^{86}Sr$ values were recalculated for 338 Ma, which is the best estimate for the emplacement age of the K1-K3 orthogneiss (U-Pb zircon ages; Kozlik et al. 2015). The complete data set of $^{87}Sr/^{86}Sr$ for scheelites, arranged according to their hosting lithologies, is graphically shown in Fig. 3. Low values of 0.72078 to 0.73625 are found in Scheelite 1 from the laminated scheelite-quartz ore (FT-74) in the eastern ore field. In contrast, $^{87}Sr/^{86}Sr$ of Scheelite 1 from the scheelite-rich gneiss (FS-1) range between 0.72887 and 0.76417 and match the isotopic composition of Scheelite 2 in the K1-K3 orthogneiss (0.72266–0.76375). Scheelite 2 in the meta-quartz diorite shows the strongest variation (0.70724–0.76832), whereas Scheelite 2 from a quartz-scheelite vein is characterised by generally high radiogenic values (0.75392–0.76812).

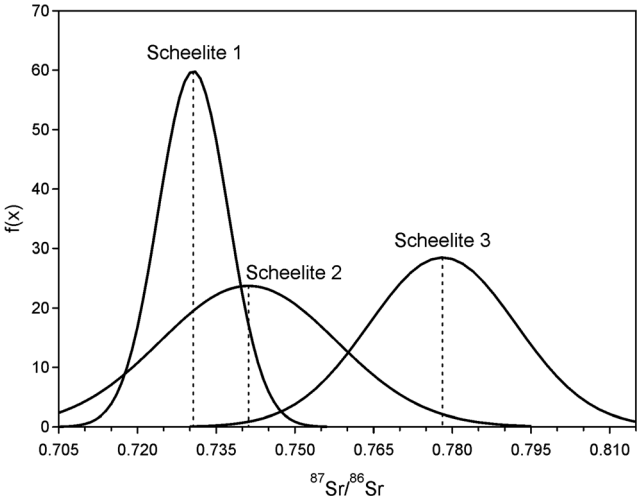

Fig. 4 $^{87}Sr/^{86}Sr$ values of Scheelite 1, 2 (without AP-3.82), and 3 (without FS-1) fitted with a Gaussian distribution. The difference in the medians between the three generations is statistically significant as tested with a Wilcoxon signed-rank test. The dashed lines represent the median value of each generation

Interestingly, Scheelite 2 (<1 mm) from a network of quartz-scheelite veinlets crosscutting the Younger K2 orthogneiss

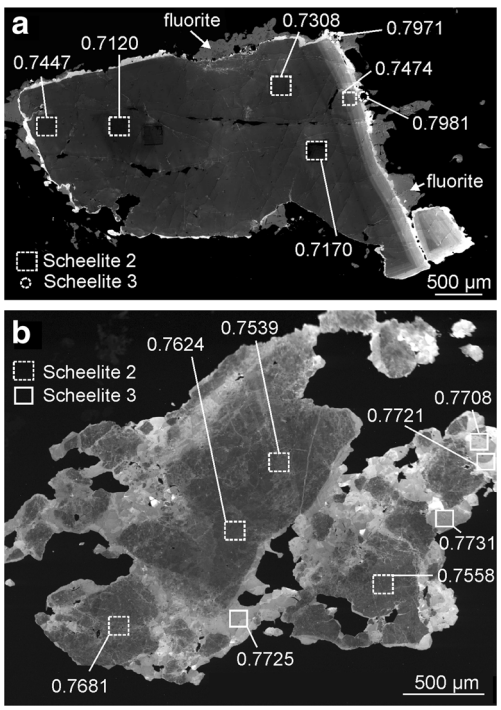

Fig. 5 Scheelite 2 crystal overgrown by Scheelite 3 documenting intragrain variation of $^{87}Sr/^{86}Sr$ within scheelite. **a** CL image of a zoned Scheelite 2 crystal from the meta-quartz diorite, sample Gn-1038a, level 1038 m, western ore field. Only the thin CL-bright outermost rim is Scheelite 3. The outermost medium grey rim is fluorite. Darker square micro-domains (outlined) are laser ablation pits with a length of 188 µm (inner parts, scheelite 2) and 104 µm (outer rim, Scheelite 3), respectively. **b** CL image of CL-dark Scheelite 2 partly recrystallised to CL-brighter Scheelite 3; scheelite-quartz vein crosscutting the K1-K3 orthogneiss, sample B-K1q-A, level 1164 m, western ore field

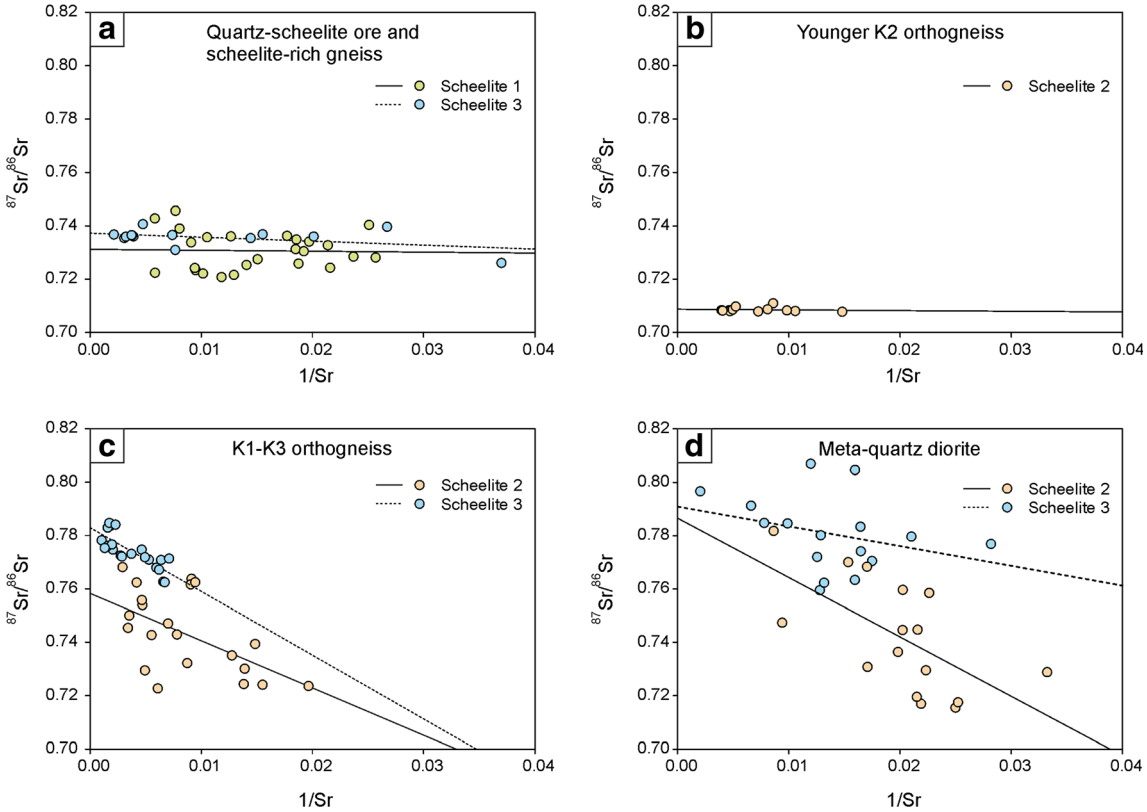

Fig. 6 **a-d** $^{87}Sr/^{86}Sr$ vs 1/Sr plots for the different scheelite generations according to their hosting lithology

(AP-3.82) displays the least radiogenic $^{87}Sr/^{86}Sr$ values of 0.70775 to 0.71093 and a smaller variation compared to the other samples. Scheelite 3 in the scheelite-rich gneiss yields $^{87}Sr/^{86}Sr$ between 0.72610 and 0.76320, which is generally lower than ratios in the respective generation from the K1-K3 orthogneiss (0.72383–0.80479), meta-quartz diorite (0.74331–0.80689) and quartz-scheelite vein (0.77079–0.77310). The $^{87}Sr/^{86}Sr$ ratio in scheelite from the Granatspitz gneiss (ST-03/30) is, with exception of one outlier (0.77467), in the range of 0.74387–0.74523 (median 0.74422). The two analyses on scheelite from the Felbertauern augengneiss (SP-25/34) yield radiogenic $^{87}Sr/^{86}Sr$ ratios of 0.77348 and 0.77366.

Summarising the results for the three investigated scheelite generations at Felbertal W deposit: $^{87}Sr/^{86}Sr$ values range between 0.72078 and 0.76417 in Scheelite 1 (median $^{87}Sr/^{86}Sr = 0.73063$) and between 0.70724 and 0.76832 in Scheelite 2 (median $^{87}Sr/^{86}Sr = 0.74283$). Thus, $^{87}Sr/^{86}Sr$ values of Scheelite 1 and 2 overlap considerably, although higher values are to be found in Scheelite 2; except Scheelite 2 from the Younger K2 orthogneiss (0.70775–0.71093). Values for Scheelite 3 are even higher, they range from 0.72383 to 0.80689 (median $^{87}Sr/^{86}Sr = 0.77532$). Scheelite 3 from the scheelite-rich gneiss is also exceptional because of relatively low and less scattering $^{87}Sr/^{86}Sr$ (median 0.73646).

Applying the Wilcoxon signed-rank test to compare the Sr isotope dataset (Fig. 4) indicates that there are statistically significant differences among the median values of the three scheelite generations. The difference between Scheelite 1 and 2, however, is not very pronounced ($P = 0.011214$) and the two datasets overlap to a great extent. Scheelite 2 from sample AP-3.82 and Scheelite 3 from sample FS-1 were not included since their $^{87}Sr/^{86}Sr$ ratios are rather low and these data are regarded as outliers (see discussion). There is also some overlap between Scheelite 2 and 3 but the median values are significantly different ($P \leq 0.000001$).

Because Scheelite 1 had been interpreted as an older generation of Cambrian age (Eichhorn et al. 1997) $^{87}Sr/^{86}Sr$ of Scheelite 1 was also recalculated to 520 Ma. Results yielded variations in the 3rd decimal place, even for analyses having the highest $^{87}Rb/^{86}Sr$. This variation is negligible considering the total variation in $^{87}Sr/^{86}Sr$ of Scheelite 1 data set and our interpretations given below are not biased in this respect.

To evaluate the spatial distribution of the Sr isotopic composition within single scheelite crystals, multiple spot analyses on larger scheelite grains were carried out. The Scheelite 2 crystal (<5 mm) from the meta-quartz diorite (Gn-1038a) reveals a remarkable scatter in its Sr isotopic systematics on a sub-mm scale with $^{87}Sr/^{86}Sr$ ratios ranging from 0.71695 to 0.74740 (Fig. 5a). The thin rim of Scheelite 3 overgrowing Scheelite 2 is even more radiogenic with $^{87}Sr/^{86}Sr$ ratios of 0.79712 and 0.79813. Furthermore, a Scheelite 2 porphyroclast from a quartz-scheelite vein (B-

K1q-A) with evidence of incomplete recrystallisation to Scheelite 3 shows $^{87}Sr/^{86}Sr$ ratios in the range of 0.75392 to 0.76812 (Fig. 5b). The Sr isotopic composition of Scheelite 3 in this sample is slightly more radiogenic but exhibits less scattering compared to Scheelite 2; $^{87}Sr/^{86}Sr$ ratios vary between 0.77079 and 0.77310.

Rb-Sr data of apatite

Data of zoned apatite from the K1-K3 orthogneiss and apatite cores from the scheelite-rich gneiss in the eastern ore field are reported and compared with data from the barren meta-quartz diorite (Gn-1262) and two Early Carboniferous Zentralgneis samples (Felbertauern augengneiss and Knorrkogel gneiss). The data are listed in Table 2. Apatite $^{87}Sr/^{86}Sr$ values, arranged according to their hosting lithologies, are shown in Fig. 3. The complete dataset is available as Electronic supplementary material (Electronic appendix 1).

In general, apatite from the studied samples shows higher Sr concentrations than scheelite, though the Sr contents differ among the samples. With regard to the median Sr concentrations, apatite cores from the K1-K3 orthogneiss (427 ppm Sr) are similar to those from the barren Knorrkogel gneiss (478 ppm Sr). Lower contents were measured in apatite cores from the scheelite-rich gneiss (202 ppm Sr) and the Felbertauern augengneiss (246 ppm Sr). The Sr concentrations in apatite rims of the K1-K3 orthogneiss (Gn-1065b, K1-725, K1-1100, K1-1152) range from 162 to 1296 ppm Sr, with a median value of 679 ppm Sr. Apatite cores from the meta-quartz diorite (Gn-1262) have Sr concentrations between 892 and 1274 ppm Sr (median 1173 ppm); the respective rims have similar contents ranging from 944 to 1248 ppm Sr (median 1105 ppm).

Because of the low $^{87}Rb/^{86}Sr$ of all apatite analyses (55 analyses with $^{87}Rb/^{86}Sr < 0.07510$; Table 2), a time-correction for calculating the initial $^{87}Sr/^{86}Sr$ ratio is not necessary. The measured $^{87}Sr/^{86}Sr$ values in apatite cores from the K1-K3 orthogneiss are highly radiogenic and range from 0.72044 to 0.74514 (median $^{87}Sr/^{86}Sr = 0.72549$). Apatite cores in the scheelite-rich gneiss also show a large variation, with initial $^{87}Sr/^{86}Sr$ ratios ranging from 0.72264 to 0.73845 (median $^{87}Sr/^{86}Sr = 0.73377$). Apatite cores from the meta-quartz diorite (Gn-1262) from the western ore field have lower initial $^{87}Sr/^{86}Sr$ values of 0.70527 to 0.70672 (median $^{87}Sr/^{86}Sr = 0.70586$), similar to apatite from the Knorrkogel gneiss with values of 0.70649 to 0.70896 (median $^{87}Sr/^{86}Sr = 0.70790$). The $^{87}Sr/^{86}Sr$ ratios in apatites from the Felbertauern augengneiss scatter and are more radiogenic with ratios ranging between 0.71634 and 0.72954 (median $^{87}Sr/^{86}Sr = 0.72192$). Compositions of apatite cores in the scheelite-rich gneiss and in the K1-K3 orthogneiss overlap with Scheelite 1 and 2, although the isotopic composition of apatite is less variable and commonly lower than in the corresponding scheelite.

Apatite rims from the K1-K3 orthogneiss have $^{87}Sr/^{86}Sr$ between 0.74535 and 0.77937 (median $^{87}Sr/^{86}Sr = 0.77211$), those from the meta-quartz diorite also show more radiogenic $^{87}Sr/^{86}Sr$ values of 0.70833 to 0.71061 (median $^{87}Sr/^{86}Sr = 0.70899$). In summary, apatite rims are consistently more radiogenic than the cores. There is no systematic correlation of increasing $^{87}Sr/^{86}Sr$ ratios from core to rim with the absolute Sr concentrations in apatite cores and rims where measured in a single crystal. Analyses of one apatite in sample K1-1100 reveal a decrease in Sr concentrations from core to rim, while in apatite from sample K1-725 Sr concentrations are similar between cores and rims.

Discussion

Radiogenic Sr isotopic signature of the Felbertal tungsten deposit

The study of Sr isotope systematics of scheelite from the Felbertal W deposit goes back to von Quadt (1985) who already reported a heterogeneous distribution of $^{87}Sr/^{86}Sr$ ratios in the different scheelite generations. The first evidence for the Early Carboniferous age of the K1-K3 orthogneiss comes from an Rb-Sr isochron age (Pestal 1983). Further Sr isotope data of scheelite and representative host rocks were published by Eichhorn et al. (1997). All these previous studies were done by conventional Sr isotope analysis on mineral separates and whole rocks. As documented in these studies, measured initial $^{87}Sr/^{86}Sr$ ratios of scheelite are exceedingly radiogenic and show remarkable scattering, ranging from 0.726 to 0.740 in Scheelite 1, 0.721 to 0.794 in Scheelite 2, 0.718 to 0.799 in Scheelite 3, and 0.721 to 0.792 in Scheelite 4. Additionally, $^{87}Sr/^{86}Sr$ ratios for one clinopyroxene relic (0.707) surrounded by tschermakitic- to magnesio-hornblende (0.736) in a hornblendite from the eastern ore field, have been reported. Calculations based on $^{87}Rb/^{86}Sr$ ratios in the range of 17.43 and 27.90 yielded time-corrected (336 Ma) initial whole rock $^{87}Sr/^{86}Sr$ ratios for the W mineralised Early Carboniferous K1-K3 orthogneiss between 0.704 and 0.708. A similar value of 0.708 is given for the Early Palaeozoic K2 orthogneisses. Only the fine-grained amphibolites and hornblendites show elevated initial $^{87}Sr/^{86}Sr$ ratios (calculated for 520 Ma) of 0.708 to 0.713 and 0.754 to 0.780, respectively.

The results of our in-situ Sr isotopic analyses correspond with those reported by Eichhorn et al. (1997) in that $^{87}Sr/^{86}Sr$ in scheelite from Felbertal show remarkable scattering within each generation and evolve towards unusual radiogenic values. Keeping in mind that this previous Sr isotope study was done conventionally, including physical/manual separation of scheelite, it was so far unclear to what extent the large

variation and overlap in the Sr isotope data of Scheelite 1 to 3 reflects mixing of scheelite generations. As documented in the Sample description there is an intimate textural intergrowth of Scheelite 3 with stages 1, respectively 2.

Generally, numerous processes were invoked to explain Sr isotopic heterogeneities in various magmatic or hydrothermal systems. These include (1) an increase of $^{87}Sr/^{86}Sr$ ratios due to proceeding magmatic differentiation of a high Rb/Sr melt during a long time span of crystallisation (Sallet et al. 2000). (2) fractional crystallisation under open-system conditions and mixing of isotopically different sources (Bizzarro et al. 2003; Tsuboi 2005). (3) mixing of magmatic fluids with externally derived (meteoric) fluids (Lüders et al. 2009). (4) modification of the $^{87}Sr/^{86}Sr$ ratio in hydrothermal fluids during infiltration of chemical heterogeneous lithologies (Bau et al. 2003; Farmer and DePaolo 1987; Kempe et al. 2001; Mueller et al. 1991). (5) incongruent release of ^{87}Sr into fluids caused by selective mineral breakdown reactions during fluid-rock interaction (Glodny and Grauert 2009). The last two processes involve hydrothermal fluids whose Sr isotopic composition is controlled by the transfer of ^{87}Sr from the host rocks interacting with the mineralising fluids.

Purely magmatic models, like the one involving longer lasting magmatic fractional crystallisation of an ^{87}Rb-enriched melt cannot explain the enormous Sr isotope variation and highly radiogenic composition of Felbertal scheelites. If the Sr isotopic signature of the hydrothermal fluids were to exclusively reflect the composition of the granitic melt from which they had exsolved, the bulk rock $^{87}Sr/^{86}Sr$ initial values of the K1-K3 orthogneiss should be much higher ($^{87}Sr/^{86}Sr > 0.72$; Fig. 3) than the reported values (0.704 and 0.708, Eichhorn et al. 1997). Such high and variable $^{87}Sr/^{86}Sr$ initial values do not conform to the metaluminous to slightly peraluminous I-type granite characteristics of the K1-K3 orthogneiss protolith (Kozlik and Raith 2014). Thus, other late to post-magmatic processes involving aqueous fluids, which were enriched in radiogenic Sr have to be considered. In the next sections we discuss that the observed Sr isotope composition of scheelite and apatite is the combined effect of magmatic, ore forming hydrothermal as well as regional metamorphic processes. A graphical presentation summarising the evolution of Sr isotopes in scheelite and apatite in the Felbertal W deposit is illustrated in Fig. 7.

Strontium isotope characteristics of the scheelite-forming magmatic-hydrothermal fluid

The large variation in $^{87}Sr/^{86}Sr$ in Scheelite 1, 2 reflects the changing Sr isotope composition of the mineralising fluids. Scheelite precipitated from fluids, which continuously or episodically experienced a modification in their Sr isotopic composition. Fluid-rock interaction and alteration of the host rocks by granite-derived hydrothermal fluids seems to be a likely explanation for the observed ^{87}Sr enrichment. Preferential leaching of high-Rb/Sr minerals, like biotite or muscovite from the Early Palaeozoic lithologies hosting the W deposit, may have contributed to the solute budget of the granite-derived fluids and shifted the Sr isotopic signature towards a more radiogenic composition. Micas from rocks of the Habach Complex are approximately 180 Ma older than the Early Carboniferous K1-K3 orthogneiss and W mineralisation, allowing for enough time to accumulate the necessary high concentrations of ^{87}Sr.

Interestingly, variations of the Sr isotope composition are also documented on the grain scale. A large (5 mm) zoned Scheelite 2 crystal shows a considerable intra-grain Sr isotopic

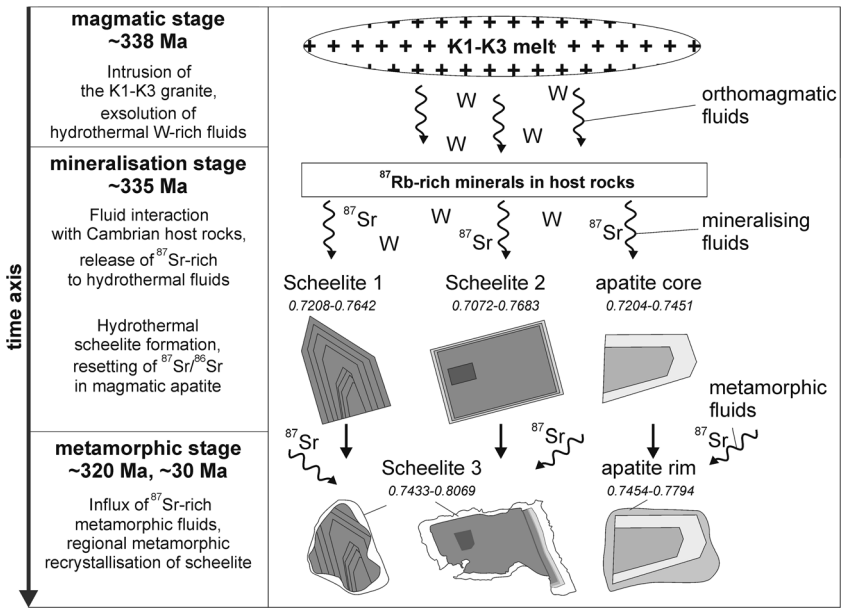

Fig. 7 Schematic sketch illustrating the Sr isotopic evolution of scheelite and apatite with time. $^{87}Sr/^{86}Sr$ values are shown in italics

variation with increasing $^{87}Sr/^{86}Sr$ from the inner zone towards the rims (Fig. 5a): the thin overgrowths of metamorphic Scheelite 3 are even more radiogenic (>0.79). The well-preserved zoning and the sudden jump in isotope composition between hydrothermal Scheelite 2 and metamorphic Scheelite 3 suggest that the metamorphic overprint did *not* change/re-equilibrate the isotopic composition of Scheelite 2. The documented within-grain variation of Scheelite 2 indicates disequilibrium conditions during (continuous or episodic) growth of scheelite from the hydrothermal fluid. In this specific case the fluid became more radiogenic with time.

The observed $^{87}Sr/^{86}Sr$ ratios of Scheelite 1 and 2 do not reflect the Sr isotopic signature of the granitic source rock from which the magmatic-hydrothermal fluids were derived, but can be best explained with fluid-rock interaction. It is hypothesized that the initial magmatic-hydrothermal fluids were characterised by lower $^{87}Sr/^{86}Sr$ ratios but became more radiogenic with progressive hydrothermal alteration. Radiogenic Sr released from Rb-rich minerals like biotite in the Early Palaeozoic host rocks could be a possible source (cf., Zuddas et al. 1995).

The variable distribution of $^{87}Sr/^{86}Sr$ in Scheelite 1 and 2 (Fig. 3) indicate several phases or pulses of mineralisation; e.g., repeated infiltration of fresh batches of hydrothermal fluid with differing Sr isotopic composition. The new in-situ data therefore document a highly dynamic hydrothermal system forming the Felbertal scheelite deposit, involving fluids of changing Sr isotopic composition with time and space.

The $^{87}Sr/^{86}Sr$ ratio and the Sr concentration in Scheelite 1 do not correlate with each other. This is illustrated in Fig. 6a, where the data points are aligned along a horizontal regression line, indicating that the isotopic composition cannot be explained with binary mixing of two isotopic distinct reservoirs. Because the laminated scheelite-quartz ore contains very few mica and feldspars, we think that in this case, the Sr signature is not controlled by the immediate "quartzitic" host rock but that the hydrothermal fluid attained its radiogenic isotope signature prior to the infiltration of this lithology.

Scheelite 2 in the leucocratic Younger K2 orthogneiss (AP-3.82) having the lowest and least scattering $^{87}Sr/^{86}Sr$ (Fig. 3) also shows a horizontal data distribution (Fig. 6b). A possible explanation could be that the plagioclase-dominated mineral assemblage of this gneiss buffers the Sr isotopic composition of the influxing magmatic-hydrothermal fluid (and consequently of the precipitating scheelite).

In contrast, Scheelite 2 from the K1-K3 orthogneiss and the meta-quartz diorite record mixing of Sr from different reservoirs (Fig. 6c, d). However, if mixing is accepted as the primary process controlling the isotopic composition of these scheelites, the scatter of the data suggests that the isotopic composition of Scheelite 2 is not only the result of a simple two-component mixture; e.g., of Sr of a magmatic hydrothermal fluid of granitic origin and Sr from Rb-rich host rock minerals. It is probable that additional factors such as the respective local abundances and the isotopic composition of feldspars, micas, and presence of other Rb-Sr-rich minerals in the host rocks interacting with the magmatic-hydrothermal fluid account for the heterogeneous Sr isotopic composition.

Interpretation of Sr isotope data of apatite

Similar to scheelite, the Sr isotope composition of apatite cannot be explained with a purely magmatic origin. The highly radiogenic $^{87}Sr/^{86}Sr$ ratios of apatite cores, as best documented for the K1-K3 orthogneiss, can be interpreted in two ways. (1) They are of magmatic origin but their pristine isotope composition had been subsequently changed. (2) Apatite cores are of hydrothermal origin. The oscillatory zoning observed in some apatite grains (Fig. 2h) is ambiguous for deciding on the origin of apatite. It resembles zoning as known from magmatic zircon but it is also similar to the zoning pattern of hydrothermal minerals, i.e. Scheelite 1 (Fig. 2a). Because apatite is the only phosphate mineral in the studied metagranitoids and it has been observed as inclusions in magmatic allanite and zircon we interpret the cores as magmatic apatite, which had changed its Sr isotope composition during post-magmatic processes.

The Sr isotope system of apatite in fluid-absent systems records diffusional exchange and redistribution between different Sr-bearing minerals (Glodny et al. 2008). In hydrothermal environments apatite may change its Sr isotope composition by interacting with the fluid, even at low temperatures (Romer 1996; Glodny et al. 2008). Accordingly, the enrichment of radiogenic ^{87}Sr in apatite cores of the K1-K3 orthogneiss is most probably related to a subsolidus fluid-crystal exchange of Sr.

The fact that the barren meta-quartz diorite on the 1262 m level in the western ore field still preserves its low (0.70527–0.70672) primary magmatic (?) values, though being of about the same age as the K1-K3 orthogneiss illustrates that interaction of the ^{87}Sr-rich fluid with the various lithologies within the deposit must have been selective.

To evaluate if the increase in radiogenic Sr in apatite and the large scatter in Sr isotopic composition is restricted to the Felbertal deposit or also seen on the regional scale two samples of the barren Knorrkogel gneiss (FB-09/30) and Felbertauern augengneiss (FB-12/30, SP-25/34) were studied. $^{87}Sr/^{86}Sr$ values of apatite cores from the Felbertauern augengneiss are similar to the K1-K3 orthogneiss (Fig. 3) suggesting that apatite in the Felbertauern augengneiss records the same hydrothermal alteration with ^{87}Sr increase as the mineralised lithologies within the Felbertal W deposit. This finding supports the proposed genetic link between the two orthogneisses, which had already been suggested based on geochemical and geochronological data (Kozlik et al. 2015). Apatites of the Knorrkogel gneiss have constantly lower and

homogeneous $^{87}Sr/^{86}Sr$ ratios comparable to apatites from the barren meta-quartz diorite (Gn-1262) indicating that highly radiogenic and scattering $^{87}Sr/^{86}Sr$ values are characteristic for W mineralisation at Felbertal associated with the K1-K3 orthogneiss. Another aspect which has influenced the Sr isotopic composition of scheelite and apatite that must be considered is metamorphism; this will be discussed in the next section.

Effects of metamorphism on the Sr isotope system

It can be shown that Scheelite 3 always has higher $^{87}Sr/^{86}Sr$ than any of the two earlier scheelite stages (Figs. 3, 7). From its textural features Scheelite 3 is interpreted as metamorphic, formed by recrystallisation and local mobilisation of pre-existing Scheelite 1 or 2 (see above). The same holds true for apatite; apatite rims are always more radiogenic than the respective cores. This is explained by the intake of radiogenic ^{87}Sr into Scheelite 3 and apatite rims from an ^{87}Sr-enriched metamorphic fluid.

Release of ^{87}Sr from breakdown of micas has already been interpreted to be responsible for the high $^{87}Sr/^{86}Sr$ of Scheelite 3 (Höll and Eichhorn 2000). A further source for ^{87}Sr, in addition to metamorphic fluid, is the pre-existing scheelite and apatite itself that undergoes recrystallisation. Trace elements and isotopes released during this process may contribute to the amount of dissolved species in the metamorphic fluid. In cases when pure recrystallisation of local scheelite material is the predominant process, the isotopic composition of Scheelite 3 remains unchanged and even becomes better homogenised. This seems to be the case for scheelite from the eastern ore field (sample FS-1; Figs. 3 and 6a). Obviously, in this case we are dealing with very *local* metamorphic isotopic equilibration of scheelite without addition of radiogenic Sr by metamorphic fluids. In other cases when ^{87}Sr was added during metamorphic recrystallisation of scheelite, the Sr isotopic signature of the metamorphic scheelite generation becomes more radiogenic. In the K1-K3 orthogneiss and meta-quartz diorite Sr isotope composition of Scheelite 3 can be considered as a mixture of Sr from different reservoirs (Fig. 6c, d).

The higher total Sr concentrations in Scheelite 3 compared to Scheelite 1 and 2 (Table 2) indicate breakdown of Sr-bearing phases during metamorphism. One possible source of Sr would be (magmatic?) plagioclase. Plagioclase breakdown (e.g., through sericitization) would increase the Sr and Ca concentrations of the metamorphic fluid, but would at the same time reduce its $^{87}Sr/^{86}Sr$ (Glodny and Grauert 2009). To account for the high $^{87}Sr/^{86}Sr$ of Scheelite 3 and the apatite rims in the K1-K3 orthogneiss and the meta-quartz diorite, we think that ^{87}Sr liberated from Rb-rich micas must also have contributed in addition to plagioclase. Thus, the Sr isotopic composition of Scheelite 3 in the K1-K3 orthogneiss and the meta-quartz diorite (Fig. 6c, d) is controlled by mixing, at varying proportions, of an already heterogeneous hydrothermal reservoir having lower but quite variable Sr concentration and isotope composition (Scheelite 2, apatite core) with a metamorphic fluid characterised by higher Sr contents and the highest $^{87}Sr/^{86}Sr$. As already pointed out above, the hydrothermal reservoir was quite heterogeneous with respect to its $^{87}Sr/^{86}Sr$.

Another aspect that needs to be discussed is the timing of the regional metamorphic overprint of Felbertal deposit. Regional metamorphism in the Tauern Window is polyphase, the dominant event being Late Eocene/Oligocene. For the Felbertal deposit it was, however, proposed that the predominant regional metamorphism is of Variscan age. A major support for the latter idea comes from Sm-Nd dating of scheelite and Re-Os dating of molybdenite. Scheelite 3 yielded a Sm-Nd isochron age of 319 ± 34 Ma (Eichhorn et al. 1997). Re-Os dating of molybdenite yielded model ages between 336 and 358 Ma and a weighted mean age of 340.3 ± 2.2 Ma (Raith and Stein 2006). Because some molybdenite is the product of the metamorphic breakdown of Mo bearing scheelite (Schenk 1990; Raith and Stein 2006) some molybdenite ages were interpreted as metamorphic (Raith and Stein 2006). It is important to note that no Alpine Re-Os molybdenite ages have been recorded.

Eichhorn et al. (1997) published a Rb-Sr isochron age of 30 ± 1 Ma for the K1-K3 orthogneiss by regressing apatite, fluorite, garnet, potassium feldspar and bulk rock Sr isotopic data, which they related to the young Alpine metamorphic overprint. Recalculation of $^{87}Sr/^{86}Sr$ for t = 30 Ma of their data yield $^{87}Sr/^{86}Sr$ of 1.30370 for biotite, 0.75562 for muscovite, 0.78065 for apatite, 0.77894 for fluorite, 0.77933 for garnet, 0.77674 for potassium feldspar, and 0.78056 for the bulk rock. Hence, a significant isotopic disequilibrium is recorded between the micas – particularly biotite – and the other minerals of the K1-K3 orthogneiss at the time of Alpine metamorphism. This suggests an incomplete resetting of the Rb-Sr system in micas from the K1-K3 orthogneiss during the youngest (i.e., Late Alpine) metamorphic overprint.

The similarities in $^{87}Sr/^{86}Sr$ of apatite rims (median $^{87}Sr/^{86}Sr = 0.77211$) and Scheelite 3 (median$^{87}Sr/^{86}Sr = 0.77532$) with the aforementioned values of non-mica minerals from the K1-K3 orthogneiss may indicate that the Sr isotopic system in Scheelite 3 and apatite rims was also affected by Sr redistribution during Alpine regional metamorphism.

Rare scheelite in the Granatspitz gneiss and the Felbertauern augengneiss reveal elevated $^{87}Sr/^{86}Sr$ ratios comparable to metamorphic Scheelite 3 from the Felbertal W deposit. Hence, in combination with their Mo poor composition (blue fluorescence) scheelite in these orthogneisses outside the Felbertal deposit is also interpreted as a product of Variscan (?) metamorphism.

Implications on the genetic model

In order to explain the highly radiogenic Sr isotope signature of the fine-grained amphibolites and scheelite Eichhorn et al. (1997) and Höll and Eichhorn (2000) proposed influx of ^{87}Sr rich crustal fluids produced by dehydration reactions in the middle to lower continental crust into a mafic magma chamber of the Habach Complex. In the hornblendite protoliths - interpreted as mafic cumulates formed at the bottom of this magma chamber - these fluids should have caused subsolidus formation of tschermakitic hornblende ($^{87}Sr/^{86}Sr = 0.740$) by replacing magmatic clinopyroxene ($^{87}Sr/^{86}Sr = 0.707$). The elevated bulk rock $^{87}Sr/^{86}Sr$ values of the fine-grained amphibolites ($^{87}Sr/^{86}Sr = 0.708–0.713$), which contrast with the low initial bulk rock $^{87}Sr/^{86}Sr$ of the Early Carboniferous K1-K3 orthogneiss ($^{87}Sr/^{86}Sr = 0.704–0.708$; Eichhorn et al. 1997) were used as one of the main arguments for a distinct pre-Variscan Early Palaeozoic mineralisation event. The second stage of scheelite mineralisation (Scheelite 2), related to the Early Carboniferous K1-K3 orthogneiss, has been assumed to be the product of assimilation/mobilisation of W from pre-existing mineralisation (Höll and Eichhorn 2000). Subsequent Variscan and Alpine regional metamorphism overprinted the older scheelite mineralisation and induced further remobilisation and redistribution of scheelite (Scheelite 3, 4).

The $^{87}Sr/^{86}Sr$ ratios of apatite cores from the studied K1-K3 orthogneiss match those of Scheelite 1 from the laminated scheelite-quartz ore. Together with the even more radiogenic Sr isotopic composition of apatite from the scheelite-rich gneiss in the eastern ore field, our new Sr isotope data indicate that the K1-K3 orthogneiss had experienced the *same* hydrothermal ^{87}Sr alteration as the Early Palaeozoic lithologies of the Habach Complex. To our opinion, the observed Sr isotope composition of Scheelite 1 and 2 can be explained more easily with a *single* magmatic-hydrothermal mineralisation event that affected all these lithologies. According to our preferred genetic model (Fig. 7), W mineralisation is linked to chemically evolved granitic melts as represented by the Early Carboniferous K1-K3 orthogneiss. Increasing magmatic differentiation concentrated the residual melt in incompatible elements (W, Nb, Ta, etc.). Siliceous fluids exsolved from these melts scavenged W and subsequently interacted with various Cambrian lithologies of the Habach Complex where they leached ^{87}Rb-rich minerals that contributed to the ^{87}Sr budget of the magmatic-hydrothermal fluids. Subsequent hydrothermal formation of primary scheelite generations 1 and 2 occurred during this mineralisation stage at ~335 Ma. As evidenced by the high $^{87}Sr/^{86}Sr$ of former magmatic apatite cores in the K1-K3 orthogneiss, the K1-K3 orthogneiss itself was strongly affected by these ^{87}Sr-enriched mineralising fluids. Subsequent Variscan (~320 Ma) and Alpine (~30 Ma) regional metamorphic events caused recrystallisation of hydrothermal scheelite and formation of metamorphic scheelite generations. The higher $^{87}Sr/^{86}Sr$ values in Scheelite 3 and apatite rims indicate influx of ^{87}Sr-rich metamorphic fluids.

Conclusions

1) In-situ LA-MC-ICP-MS studies of Sr isotopes on scheelite and apatite from the Felbertal W deposit indicate a dynamical magmatic-hydrothermal environment in which the Sr isotopic composition of the mineralising fluids changed over time. Interaction with Rb-rich Early Palaeozoic host rocks of the Habach Complex contributed to the solute budget of the magmatic-hydrothermal fluids exsolved from the crystallising K1-K3 melt. No isotopic equilibrium prevailed during subsequent precipitation of scheelite from these hydrothermal fluids as indicated by the remarkable scatter in $^{87}Sr/^{86}Sr$ of hydrothermal scheelite (Scheelite 1 and 2). Isotopic disequilibrium is documented even on the sub-mm scale by the intra-grain variation of $^{87}Sr/^{86}Sr$ in Scheelite 2.
2) The Sr isotopic composition of magmatic apatite cores from the K1-K3 orthogneiss was equally modified during the hydrothermal mineralisation processes, what is *not* reflected in the initial bulk rock $^{87}Sr/^{86}Sr$ values of the orthogneiss. The scattering and strongly radiogenic $^{87}Sr/^{86}Sr$ values in scheelite and apatite are consistent with a single-phase genetic model in which the W mineralisation at Felbertal is linked to the intrusion of the K1-K3 metagranitoid during the Early Carboniferous.
3) The subsequent regional metamorphic overprint of the W deposit causing redistribution of ^{87}Sr and the further increase in $^{87}Sr/^{86}Sr$ is also documented in the metamorphic Scheelite 3 generation and in apatite rims.

Acknowledgments We are grateful to Linda Marko for assistance with sample separation, preparation of mounts and help with isotope analyses. Helmut Mühlhans is thanked for preparation of polished (thin) sections. Marie-Luise Pecher and Steffen Schmidt from Wolfram Bergbau und Hütten AG (WBH AG) are thanked for their support during fieldwork and sampling. The management of WBH AG is thanked for enabling access to the Felbertal deposit and permission to publish data of this joint project. The constructive reviews by Gerhard Franz and Paul Nex have significantly contributed to improve the manuscript. Associate Editor Dirk Frei and Editor-in-Chief Lutz Nasdala are thanked for editorial handling of the manuscript. This project is financed by the Austrian Research Promotion Agency (FFG Bridge project 834149/30661) and WBH AG.

References

Bau M, Romer R, Lüders V, Dulski P (2003) Tracing element sources of hydrothermal mineral deposits: REE and Y distribution and Sr-Nd-Pb isotopes in fluorite from MVT deposits in the Pennine Orefield, England. Mineral Deposita 38:992–1008

Bell K, Anglin CD, Franklin JM (1989) Sm-Nd and Rb-Sr isotope systematics of scheelites: possible implications for the age and genesis of vein-hosted gold deposits. Geology 17:500–504

Bizzarro M, Simonetti A, Stevenson R, Kurszlaukis S (2003) In situ $^{87}Sr/^{86}Sr$ investigation of igneous apatites and carbonates using laser-ablation MC-ICP-MS. Geochim Cosmochim Acta 67:289–302

Briegleb D (1987) Geologische Verhältnisse im Bereich der Scheelitlagerstätte im Felbertal, Pinzgau (Land Salzburg). Uni Aktuell Salzburg 10:10–11

Briegleb D (1991) Die Scheelitlagerstätte im Felbertal bei Mittersill (Land Salzburg). Ber Dt Min Ges 2:48–50

Brugger J, Lahaye Y, Costa S, Lambert D, Bateman R (2000) Inhomogeneous distribution of REE in scheelite and dynamics of Archaean hydrothermal systems (Mt. Charlotte and Drysdale gold deposits, Western Australia). Contrib Mineral Petrol 139:251–264

Brugger J, Maas R, Lahaye Y, McRae C, Ghaderi M, Costa S, Lambert D, Bateman R, Prince K (2002) Origins of Nd–Sr–Pb isotopic variations in single scheelite grains from Archaean gold deposits, Western Australia. Chem Geol 182:203–225

Creaser RA, Gray CM (1992) Preserved initial $^{87}Sr/^{86}Sr$ in apatite from altered felsic igneous rocks: a case study from the middle Proterozoic of South Australia. Geochim Cosmochim Acta 56: 2789–2795

Darbyshire DPF, Pitfield PEJ, Campbell SDG (1996) Late Archean and Early Proterozoic gold-tungsten mineralization in the Zimbabwe Archean craton: Rb-Sr and Sm-Nd isotope constraints. Geology 24:19–22

Dostal J, Kontak D, Chatterjee AK (2009) Trace element geochemistry of scheelite and rutile from metaturbidite-hosted quartz vein gold deposits, Meguma Terrane, Nova Scotia, Canada: genetic implications. Mineral Petrol 97:95–109

Eichhorn R, Schärer U, Höll R (1995) Age and evolution of scheelite-hosting rocks in the Felbertal deposit (Eastern Alps): U-Pb geochronology of zircon and titanite. Contrib Mineral Petrol 119:377–386

Eichhorn R, Höll R, Jagoutz E, Schärer U (1997) Dating scheelite stages: a strontium, neodymium, lead approach from the Felbertal tungsten deposit, Central Alps, Austria. Geochim Cosmochim Acta 61:5005–5022

Eichhorn R, Höll R, Loth G, Kennedy A (1999) Implications of U–Pb SHRIMP zircon data on the age and evolution of the Felbertal tungsten deposit (Tauern Window, Austria). Int J Earth Sci 88:496–512

Eichhorn R, Loth G, Höll R, Finger F, Schermaier A, Kennedy A (2000) Multistage Variscan magmatism in the central Tauern Window (Austria) unveiled by U/Pb SHRIMP zircon data. Contrib Mineral Petrol 139:418–435

Eichhorn R, Loth G, Kennedy A (2001) Unravelling the pre-Variscan evolution of the Habach terrane (Tauern Window, Austria) by U-Pb SHRIMP zircon data. Contrib Mineral Petrol 142:147–162

Farmer GL, DePaolo DJ (1987) Nd and Sr isotope study of hydrothermally altered granite at San Manuel, Arizona; implications for element migration paths during the formation of porphyry copper ore deposits. Econ Geol 82:1142–1151

Finger F, Kraiger H, Steyrer HP (1985) Zur Geochemie des K1-Gneises der Scheelitlagerstätte Felbertal (Pinzgau/Salzburg) - ein Vorbericht. Der Karinthin 92:225–235

Franz C, Grundmann G, Ackermand D (1986) Rock forming beryl from a regional metamorphic terrain (Tauern Window, Austria): parageneses and crystal chemistry. TMPM Tschermaks Miner Petrogr Mitt 35:167–192

Frasl G (1958) Zur Seriengliederung der Schieferhülle in den mittleren Hohen Tauern. Jb Geol B-A 101:323–472

Ghaderi M, Palin M, Campbell IH, Sylvester PJ (1999) Rare earth element systematics in scheelite from hydrothermal gold deposits in the Kalgoorlie-Norseman region, Western Australia. Econ Geol 94: 423–438

Gilg HA, Höll R, Kupferschmied MP, Reitz E, Stärk H (1989) Die Basisschieferfolge in der Habachformation im Felber- und Amertal (Tauernfenster, Salzburg): Gesteinsinhalt, Geochemie, Fossilführung und genetische Implikationen. Mitt Österr Geol Ges 81:65–91

Glodny J, Kühn A, Austrheim H (2008) Diffusion versus recrystallization processes in Rb–Sr geochronology: isotopic relics in eclogite facies rocks, Western Gneiss Region, Norway. Geochim Cosmochim Acta 72:506–525

Glodny J, Grauert B (2009) Evolution of a hydrothermal fluid-rock interaction system as recorded by Sr isotopes: a case study from the Schwarzwald, SW Germany. Mineral Petrol 95:163–178

Grundmann G (1989) Metamorphic evolution of the Habach Formation a review. Mitt Österr Geol Ges 81:133–149

Höck V (1993) The Habach-Formation and the Zentralgneis - a key in understanding the palaeozoic evolution of the Tauern Window (Eastern Alps). In: Raumer JF, Neubauer F (eds) Pre-Mesozoic geology in the Alps. Springer, Berlin Heidelberg New York, pp. 361–374

Höll R (1975) Die Scheelitlagerstätte Felbertal und der Vergleich mit anderen Scheelitvorkommen in den Ostalpen. Verlag der Bayerischen Akademie der Wissenschaften, München

Höll R (1977) Early Palaeozoic ore deposits of the Sb-W-Hg formation. In: Klemm DD, Schneider HJ (eds) Time- and strata-bound ore deposits. Springer, Berlin Heidelberg New York, pp. 169–198

Höll R (1979) Time- and stratabound Early Paleozoic scheelite, stibnite and cinnabar deposits in the Eastern Alps. Verh Geol B-A 3:369–387

Höll R, Eichhorn R (2000) Tungsten mineralization and metamorphic remobilization in the Felbertal scheelite deposit, Central Alps, Austria. In: Spry PG, Marshall B, Vokes FM (eds) metamorphosed and metamorphogenic ore deposits. Rev Econ Geol 11:233–264

Horstwood MSA, Evans JA, Montgomery J (2008) Determination of Sr isotopes in calcium phosphates using laser ablation inductively coupled plasma mass spectrometry and their application to archaeological tooth enamel. Geochim Cosmochim Acta 72:5659–5674

Kebede T, Klötzli U, Kosler J, Skiöld T (2005) Understanding the pre-Variscan and Variscan basement components of the central Tauern Window, Eastern Alps (Austria): constraints from single zircon U-Pb geochronology. Int J Earth Sci 94:336–353

Kempe U, Belyatsky B, Krymsky R, Kremenetsky A, Ivanov P (2001) Sm–Nd and Sr isotope systematics of scheelite from the giant Au(−W) deposit Muruntau (Uzbekistan): implications for the age and sources of Au mineralization. Mineral Deposita 36:379–392

Koller F, Richter W (1984) Die Metarodingite der Habachformation, Hohe Tauern (Österreich). TMPM Tschermaks Miner Petrogr Mitt 33:49–66

Kozlik M, Raith JG (2014) Chemical characteristics of the K1-K3 metagranitoid in the Felbertal scheelite deposit (Austria). Mitt Österr Mineral Ges 160:37–42

Kozlik M, Raith JG, Gerdes A (2015) U-Pb, Lu-Hf and trace element characteristics of magmatic and hydrothermal zircon from the Felbertal scheelite deposit (Austria): new constraints on timing and source of W-mineralization. Chem Geol (in press)

Lüders V, Romer R, Gilg HA, Bodnar RJ, Pettke T, Misantoni D (2009) A geochemical study of the Sweet Home Mine, Colorado Mineral Belt, USA: hydrothermal fluid evolution above a hypothesized granite cupola. Mineral Deposita 44:415–434

Mueller AG, de Laeter JR, Groves DI (1991) Strontium isotope systematics of hydrothermal minerals from epigenetic Archean gold deposits in the Yilgarn block, Western Australia. Econ Geol 86:780–809

Neinavaie MH, Ghasemi B, Fuchs HW (1983) Die Erzvorkommen Osttirols. Veröffentlichungen des Tiroler Landesmuseums Ferdinandeum 63:69–113

Peng B, Frei R (2004) Nd-Sr-Pb isotopic constraints on metal and fluid sources in W-Sb-Au mineralization at Woxi and Liaojiaping (western Hunan, China). Mineral Deposita 39:313–327

Pestal G (1983) Beitrag zur Kenntnis der Geologie im mittleren Hohen Tauern Bereich des Amer- und Felbertals. University of Vienna, Dissertation

Raimbault L, Baumer A, Dubru M, Benkerrou C, Croze V, Zahm A (1993) REE fractionation between scheelite and apatite in hydrothermal conditions. Am Mineral 78:1275–1285

Raith JG, Stein HJ (2006) Variscan ore formation and metamorphism at the Felbertal scheelite deposit (Austria): constraining tungsten mineralisation from Re–Os dating of molybdenite. Contrib Mineral Petrol 152:505–521

Raith JG, Schmidt S (2010) Tungsten deposit Felbertal, Salzburg, Austria. Acta Mineralogica-Petrographica, Field Guide Series 3:1–24

Raith JG, Gerdes A, Cornell DH (2011) In situ U-Pb dating of scheelite: constraints on the age and genesis of the Felbertal tungsten deposit. Mineral Mag 75:1690

Rankenburg K (2002) Megacrysts in volcanic rocks of the Cameroon volcanic line – constraints of magma genesis and contamination. University of Frankfurt, Dissertation

Romer RL (1996) U-Pb systematics of stilbite-bearing low-temperature mineral assemblages from the Malmberget iron ore, northern Sweden. Geochim Cosmochim Acta 60:1951–1961

Sallet R, Moritz R, Fontignie D (2000) Fluorite $^{87}Sr/^{86}Sr$ and REE constraints on fluid-melt relations, crystallization time span and bulk D^{Sr} of evolved high-silica granites. Tabuleiro granites, Santa Catarina, Brazil. Chem Geol 164:81–92

Schenk P (1990) Mikrothermometrische gefügekundliche und geochemische Untersuchungen zur Genese der Scheelitlagerstätte Felbertal/Ostalpen. University of Munich, Dissertation

Song G, Qin K, Li G, Evans NJ, Chen L (2014) Scheelite elemental and isotopic signatures: implications for the genesis of skarn-type W-Mo deposits in the Chizhou area, Anhui province, eastern China. Am Mineral 99:303–317

Stampfli GM, Borel GD (2002) A plate tectonic model for the Paleozoic and Mesozoic constrained by dynamic plate boundaries and restored synthetic oceanic isochrones. Earth Planet Sci Lett 196:17–33

Topa D, Makovicky E, Paar WH (2002) Composition ranges and exsolution pairs for the members of the bismuthinite-aikinite series from Felbertal, Austria. Can Mineral 40:849–869

Tornos F, Galindo C, Crespo JL, Spiro BF (2008) Geochemistry and origin of calcic tungsten-bearing skarns, Los Santos, Central Iberian Zone, Spain. Can Mineral 46:87–109

Tsuboi M (2005) The use of apatite as a record of initial $^{87}Sr/^{86}Sr$ ratios and indicator of magma processes in the Inagawa pluton, Ryoke belt, Japan. Chem Geol 221:157–169

Voicu G, Bardoux M, Stevenson R, Jébrak M (2000) Nd and Sr isotope study of hydrothermal scheelite and host rocks at Omai, Guiana Shield: implications for ore fluid source and flow path during the formation of orogenic gold deposits. Mineral Deposita 35:302–314

von Quadt A (1985) Geochronologische, geochemische und isotopengeochemische Untersuchungen an Gesteinen der Habach-Formation, der Scheelitlagerstätte und des angrenzenden Altkristallins im Felbertal (Land Salzburg). Dissertation, Eidgenössische Technische Hochschule Zürich

von Quadt A (1992) U-Pb zircon and Sm-Nd geochronology of mafic and ultramafic rocks from the central part of the Tauern Window (eastern Alps). Contrib Mineral Petrol 110:57–67

Woodhead JD, Hergt JM (2001) Strontium, neodymium and lead isotope analyses of NIST glass certified reference materials: SRM 610, 612, 614. Geostand Newslett 25:261–266

Zuddas P, Seimbille F, Michard G (1995) Granite-fluid interaction at near-equilibrium conditions: experimental and theoretical constraints from Sr contents and isotopic ratios. Chem Geol 121:145–154